Effect of Aperture Feed and Reflector Configuration on the Time- and Frequency Domain Radiation Patterns of Reflector Impulse Radiating Antennas

J. Scott Tyo, *Member, IEEE*, Everett G. Farr, *Senior Member, IEEE*, Jon S. H. Schoenberg, *Senior Member, IEEE*, Leland H. Bowen, *Member, IEEE*, and Larry L. Altgilbers, *Member, IEEE*

***Abstract*—The prompt off-boresight radiation from an arbitrary reflector impulse radiating antenna (IRA) is considered in both the time and frequency domains using a time-domain physical optics formalism. The theory is used to compare the performance between reflector IRAs with common transverse electromagnetic feed configurations that have been designed to maximize the boresight fields. It is found that moving the feed arms of reflector IRAs toward the vertical helps to reduce sidelobe levels, as reflector IRAs with their feed arms oriented at 60° from the horizontal have sidelobes that are 4–5 dB lower in the H plane and 1–2 dB lower in the E plane than more traditional reflector IRAs with feed arms oriented at 45°. The lower sidelobes are accompanied by a higher peak gain, albeit with a wider beamwidth. There are corresponding significant differences in the time domain waveforms that result. The theory is verified by comparison with experimental data from a half IRA with feed arms at 45°. The peak fields, pulse widths, and overall waveform shapes agree well between theory and experiment, though there are temporal asymmetries in the measured data that are not predicted by the theory.**

***Index Terms*—Impulse radiating antennas (IRAs), physical optics, time domain electromagnetics, ultrawide-band electromagnetics, wide-band antennas.**

I. Introduction

IMPULSE radiating antenna's (IRAs) are a class of focused aperture antennas that have been used extensively for the generation and radiation of ultrawide-bandelectromagnetic pulses [1]. IRAs are comprised of a nondispersive, conically-symmetric transverse electromagnetic (TEM) structure (transmission line) feeding some sort of focusing optic. The most common types of focusing optics are reflectors and lenses. The focusing optic converts the outgoing spherical wave on the TEM feed structure into a plane wave in the near-field by the geometric optics approximation. A stereographic projection [2] is used to convert the mode structure of the conical TEM mode into a longitudinal TEM mode at the aperture plane for purposes of analysis. A schematic of a typical reflector IRA is shown in Fig. 1.

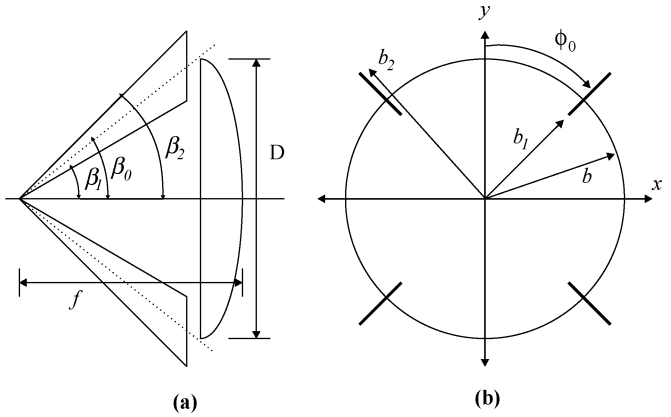

Fig. 1. Schematic of the IRA being studied. (a) Side view with focal length and diameter. (b) Aperture plane after stereographic projection.

A. Boresight Radiation

The radiated fields on boresight from an IRA can be predicted by using the distribution of the TEM mode in the focused aperture of the antenna and considering aperture theory in either the time or frequency domain. For the early time, the radiated field on boresight at position r and time t is given in the physical optics approximation as [1]

$$E_{rad} = \frac{h_a}{2\pi r c f_g}\frac{dV}{dt} \tag{1}$$

where V is the applied voltage waveform and h_a is the aperture height given as

$$h_a = \frac{f_g}{V_0}\iint_A E_y(x,y)dxdy. \tag{2}$$

In (2), $f_g = Z_{\text{line}}/\eta_0$, Z_{line} is the impedance of the TEM feed structure, $\eta_0 = 120\pi\Omega$, V_0 is the peak applied voltage, and A is the focused aperture. Equations (1) and (2) are valid for the clear time of the antenna, which is the time it takes for secondary interactions to occur and propagate to the observer, such as scattering from the feed point or the edges of the reflector. In most IRAs, the clear time is on the order of the physical size of the

Manuscript received February 27, 2003; revised June 11, 2003. This work was supported by the U.S. Army Space and Missile Defense Command.

J. S. Tyo is with the Electrical Engineering and Computer Engineering Department, University of New Mexico, Albuquerque, NM 87131 USA (e-mail: tyo@ieee.org).

E. G. Farr and L. H. Bowen are with Farr Research, Incorporated, Albuquerque, NM 87123 USA (e-mail: efarr@farr-research.com; lhbowen@farr-research.com.

J. S. H. Schoenberg was with the Air Force Research Lab/DEHP, Kirtland AFB, NM 87117 USA. He is now with the U.S. Department of Defense (e-mail: schoenberg@ieee.org).

L. L. Altgilbers is with the U.S. Army Space and Missile Defense Command, Redstone Arsenal, AL 35807 USA.

Digital Object Identifier 10.1109/TAP.2004.830256

antennas (such as D/c or f/c, depending on the exact configuration of the antenna). For the clear time of the antenna, we refer to the fields as "prompt."

An example of a TEM feed structure in the aperture plane with the corresponding E field lines is presented in Fig. 2. For a specific feed configuration, the choice of aperture A bounded by contour C has a significant effect on the prompt radiated field. Several authors have studied the effects of altering the aperture shape for a given feed structure in order to optimize the radiated field [3]–[6]. Once the feed structure and aperture outer boundary are specified, the prompt radiated field can be maximized by removing the portions of the aperture where E_y contributes destructively to the aperture integral in (2). Furthermore, an optimum ratio between the radius of the feed arms and the maximum radius of the circular aperture was calculated, and shown to be a function of both feed impedance and feed arm angle [5]. Recent numerical [6] and experimental [7] results have demonstrated that simply changing the feed arm angle to 60° (from the horizontal) from the more conventional 45° can produce an increase in aperture height of approximately 20% and a reduction by as much as 15 dB in the cross-polarized sensitivity on boresight.

While the radiated fields on boresight are well understood, relatively few investigations have focused on the radiation from these antennas in directions other than the direction of focus. Furthermore, all of the modifications discussed above were designed to maximize the boresight radiated fields, and their effects on the off-boresight fields are unknown. IRAs are known to have extremely narrow beamwidths, so knowledge of the off-boresight fields is also important to understand how the waveform changes as one moves away from the direction of focus. IRAs were designed to radiate transient electromagnetic pulses, but the nondispersive nature of IRAs and their inherently wide (multiple decades) impedance bandwidth make IRAs attractive for multi band applications such as swept CW radar and multiband communications. An understanding of the sidelobe performance is important If IRAs are to be used for such broadband CW applications.

B. IRA Configurations Examined

In this paper, we investigate the off-boresight radiated fields in the time and frequency domains for several aperture configurations that have been shown to work well for the radiation of large prompt boresight fields. The emphasis in this study is on the effect of the TEM mode distribution in the aperture plane and the corresponding choice of aperture bounding contour C. Higher order effects such as scattering from the feed arms and the edges of the reflector are not considered. The aperture configurations tested here have feed arms at either 45° or 60° from the horizontal. The 45° case is the most common configuration that has been used for manufacturing IRAs [8], but recent results have demonstrated that improvements of 20% or more in h_a are possible for a fixed feed impedance by simply moving the feed arms toward the vertical [6], [7]. For each feed arm angle, there are three aperture configurations tested, as shown in Fig. 2. The first is the most common configuration, whereby the focused aperture coincides with the circle of symmetry of the feed arms.

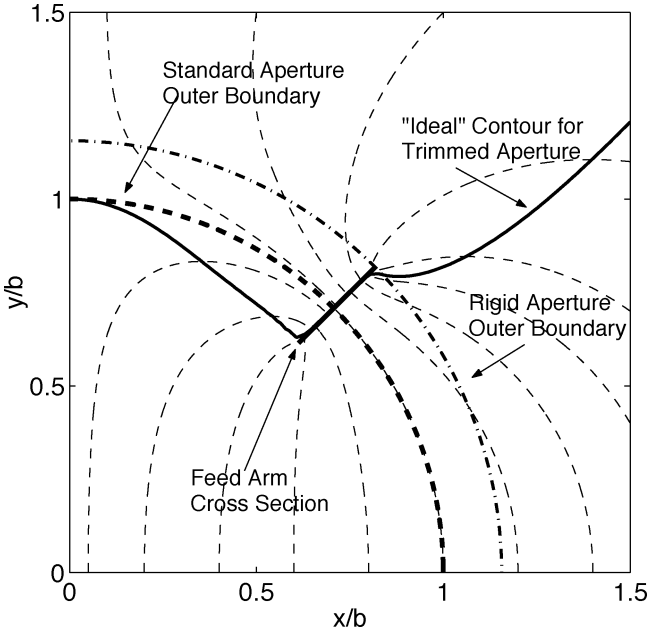

Fig. 2. Feed configuration and electric field lines for $Z_{\text{line}} = 200\ \Omega$ and $\phi_0 = 45°$. Fields are shown in the first quadrant of the $x - y$ plane, as the other quadrants can be obtained by symmetry. Also presented are the aperture contours used in this study. The standard aperture coincides with the circle of symmetry. The rigid aperture focuses the entire portion of the aperture with radius less than b_2 (see Fig. 1). The trimmed aperture has the same maximum size as the rigid aperture, only the portions above the ideal contour where E_y is oriented in the wrong direction are eliminated. The electric field lines for the TEM mode are shown as dashed lines in the figure.

We term this the "standard (S)" configuration. It has been shown that the optimal circular aperture (in the sense of aperture efficiency) is the standard aperture [5]. As can be seen in Fig. 1, the standard aperture requires that a significant portion of the feed arms be *outside* the reflector, and therefore, the feed arms must be self-supporting. In some applications where the IRA is to be a deployable antenna fabricated from fabric, the feed arms are not self supporting and mechanical considerations force the antenna to have rigid support at the outer edge of the feed arms [9], [10]. In light of this requirement, the second aperture configuration extends to the outer edge of the feed arms. We term this the "rigid (R)" configuration since the additional aperture area is needed to maintain the mechanical rigidity of the feed arms. When using such an aperture, the prompt radiated fields in (1) can be enhanced by removing the portion of the aperture where the fields contribute destructively to the integral in (2) [5]. The third aperture configuration that we test here has the same maximum aperture curve as the rigid aperture, but the portions of the aperture above the ideal contour in Fig. 2 is removed. We term this the "trimmed (T)" configuration. In practice, the trimmed configuration could be constructed by physically removing portions of the reflector. All feed configurations examined in this paper are for $Z_{\text{line}} = 200\ \Omega$, but the results are qualitatively similar for other impedances [11].

Previous studies have investigated the on-boresight, prompt performance of IRAs employing the aperture configurations discussed here both theoretically/numerically [5], [6] and experimentally [5], [7]. In the remainder of this paper, we present the theory for off-boresight radiation from an IRA and address

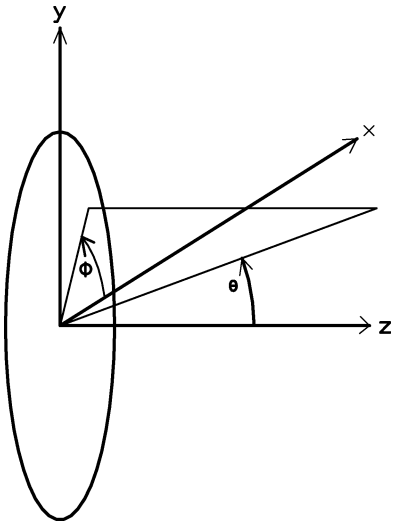

Fig. 3. Coordinates for gain/sidelobe calculations.

the impact of the proposed aperture alterations on the prompt off-boresight fields. Section II presents the physical optics formulation for the prompt radiated fields in the time domain and Section III presents the corresponding results in the frequency domain. Section IV compares the theoretical predictions with experimental results for an IRA with the standard aperture configuration. Discussion of the results is presented in Section V, and conclusions are drawn in Section VI.

II. Physical Optics Model in the Time Domain

In order to predict the early-time, off-boresight radiation from an IRA, we turn to the theory of focused aperture antennas. The following analysis could proceed in either the time domain or the frequency domain. In his original analysis for the fields in the direction of focus, Baum [12] analyzed the boresight radiation in the Laplace domain, then performed an inverse Laplace transform to predict the time domain fields. We present a direct time domain theory here that is also valid for off-boresight directions. Even though the theory developed here is based on conventional aperture theory, many of the specific results that are derived apply only to the problem of a focused aperture antenna excited by the TEM mode of a nondispersive feed structure.

The coordinates used for the focused aperture problem are shown in Fig. 3. Using conventional aperture theory [13], we can solve this problem by employing the field equivalence theorem. If we assume that the electric and magnetic fields outside the aperture are zero, we can replace the fields on the aperture plane with equivalent surface currents. In reality, the fields outside the aperture are nonzero; however, these fields are unfocused and do not contribute significantly to the prompt radiated fields. Replacing the aperture plane with a perfect electrically conducting plane allows us to use image theory and ignore the electric surface current and double the magnetic surface current in computing the radiated fields far from the antenna. The equivalent magnetic current in the aperture is given by

$$\mathbf{M}_s(x',y',t) = -2\hat{\mathbf{z}} \times \mathbf{E}_{\mathrm{TEM}}(x',y',t) \tag{3}$$

where $\mathbf{E}_{\mathrm{TEM}}$ is the electric field of the TEM mode. The primed coordinates indicate the aperture (source) point. Using the time domain Green's function for radiation in a uniform half space, the electric vector potential $\mathbf{F}$ at position $\mathbf{r}$ and time t is

$$\mathbf{F}(\mathbf{r},t) = \frac{\varepsilon}{4\pi}\iint_A \frac{\mathbf{M}_s\left(\mathbf{r}', t-\frac{R}{c}\right)}{R}dx'dy' \tag{4}$$

where $R = |\mathbf{r}-\mathbf{r}'|$ and c is the speed of light.

Using the law of cosines and the first two terms of the Taylor series, we can approximate

$$R \approx r - \sin\theta\cos\phi x' - \sin\theta\sin\phi y' \tag{5}$$

and (4) becomes

$$\begin{aligned}\mathbf{F}(\mathbf{r},t) &= \frac{\varepsilon}{2\pi r}\iint_A \left(-\hat{\mathbf{y}}E_x\left(x',y',t-\frac{r}{c}+\frac{\sin\theta\cos\phi x'+\sin\theta\sin\phi y'}{c}\right)\right.\\ &\qquad \left.+\hat{\mathbf{x}}E_y\left(x',y',t-\frac{r}{c}\frac{\sin\theta\cos\phi x'\sin\theta\sin\phi y'}{c}\right)\right)\\ &\quad \times dx'dy'. \end{aligned}\tag{6}$$

The portion of the integrand in (6) in the y direction produces the cross-polarized radiated field, and the portion of the integrand in (6) in the x direction produces the copolarized field. We will now evaluate the electric field in the E and H planes component by component.

A. Copolarized Radiation

The principal polarization from this IRA is due to the y component of the TEM mode E field, which produces a Magnetic current (and F field) that is in the x direction. The radiated $\mathbf{E}_{\mathrm{co}}$ field is obtained by taking the curl of $\mathbf{F}$ as

$$\mathbf{E}_{\mathrm{co}} = -\frac{1}{\varepsilon}\nabla\times F_x\hat{\mathbf{x}} = -\frac{1}{\varepsilon}(\nabla F_x)\times\hat{\mathbf{x}}. \tag{7}$$

The gradient of F_x is evaluated approximately as

$$\begin{aligned}\nabla F_x &\approx -\hat{\mathbf{r}}\frac{\varepsilon}{2\pi rc}\frac{d}{dt}\iint_A\\ &E_y\left(x',y',t-\frac{r}{c}+\frac{\sin\theta\cos\phi x'+\sin\theta\sin\phi y'}{c}\right)dx'dy'.\end{aligned}\tag{8}$$

Terms of degree $(1/r)^2$ or higher have been ignored to obtain the far-zone approximation in (8). The corresponding copolarized field is

$$\begin{aligned}\mathbf{E}_{\mathrm{co}} &= \frac{1}{2\pi rc}(\hat{\phi}\cos\theta\cos\phi+\hat{\theta}\sin\phi)\frac{d}{dt}\iint_A\\ &E_y\left(x',y',t-\frac{r}{c}+\frac{\sin\theta\cos\phi x'+\sin\theta\sin\phi y'}{c}\right)dx'dy'.\end{aligned}\tag{9}$$

We now use (9) to find the temporal radiated field in the E- and H planes. In the H plane we have $\phi = \{0,\pi\}$, and we compute the radiation as a function of the polar angle θ (see Fig. 3). The $\hat{\theta}$ term in (9) disappears, and the radiated E field

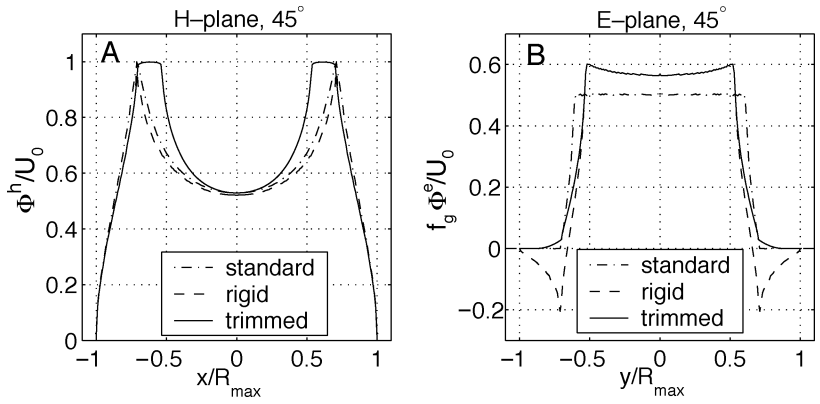

Fig. 4. (a) $\Phi^h(x)$ and (b) $\Phi^e(y)$ for the 45° feed arms, for all configurations shown in Fig. 2. The impedance is 200 Ω. The position variables are normalized to the maximum radius. For the standard aperture, the maximum radius is b (see Fig. 1). For the rigid and trimmed apertures, the maximum radius is b_2. Φ^h is normalized to the electric scalar potential difference between the feed arms. Φ^e is normalized to the total magnetic scalar potential obtained in integrating around the feed arms. This is equivalent to the total stored charge in the capacitor, and is obtained using $f_g = U_0/V_0$.

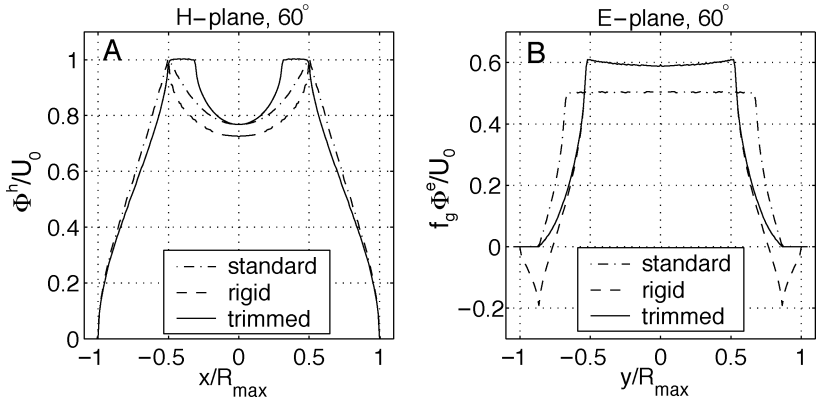

Fig. 5. (a) $\Phi^h(x)$ and (b) $\Phi^e(y)$ for the 60° feed arms, for all configurations shown in Fig. 2. The impedance is 200 Ω. The curves are prepared in the same manner as discussed in the caption of Fig. 4.

is in the $\hat{\phi}$ direction. We use $t' = t - r/c$, the retarded time at the center of the aperture, and assume ideal unit step function excitation $u(t)$ to produce

$$E_\phi^h(r,\theta,t) = \frac{\cos\theta}{2\pi rc}\frac{d}{dt}\iint_A E_y\left(x',y',t'+\frac{\sin\theta x'}{c}\right)dx'dy' \quad (10)$$

$$= \frac{\cos\theta}{2\pi rc}\frac{d}{dt}\iint_A E_y\left(x',y'\right)u\left(t'+\frac{\sin\theta x'}{c}\right)dx'dy' \quad (11)$$

$$= \frac{\cos\theta}{2\pi rc}\iint_A E_y\left(x',y'\right)\delta\left(t'+\frac{\sin\theta x'}{c}\right)dx'dy' \quad (12)$$

$$= \frac{\cot\theta}{2\pi r}\int_{y_{\min}}^{y_{\max}} E_y\left(-\frac{ct'}{\sin\theta},y'\right)dy' \quad (13)$$

where $y_{\min}$ and $y_{\max}$ are the minimum and maximum vertical extents of the aperture at a given value of x, respectively.

We define the quantity $\Phi^h(x)$ as

$$\Phi^h(x) = \left(\frac{1}{V_0}\right)\int_{y_{\min}}^{y_{\max}} E_y(x,y')dy'. \quad (14)$$

When the electric field in the aperture is a curl-free TEM mode (as is the case in IRAs), the quantity $\Phi^h(x)$ is equivalent to the electric scalar potential difference between the top and bottom of the aperture at horizontal position x. Using (14), (13) becomes

$$E_\phi^h(r,\theta,t) = \frac{V_0\cot\theta}{2\pi r}\Phi^h\left(-\frac{ct'}{\sin\theta}\right). \quad (15)$$

A similar analysis in the E plane ($\phi = \pi/2, 3\pi/2$) yields

$$E_\theta^e(r,\theta,t) = \frac{V_0}{2\pi r\sin\theta}\Phi^e\left(-\frac{ct'}{\sin\theta}\right) \quad (16)$$

where

$$\Phi^e(y) = \left(\frac{1}{V_0}\right)\int_{x_{\min}}^{x_{\max}} E_y(x',y)dx'. \quad (17)$$

When the electric field in the aperture is a TEM mode, $\Phi^e(y)$ is equivalent to the difference in magnetic scalar potential at the right and left edges of the aperture at vertical position y. The computed values of $\Phi^h(x)$ and $\Phi^e(y)$ are shown in Fig. 4 and Fig. 5 for the 200 Ω IRA with 45° and 60° feed arms. The above theory predicts that the off-boresight radiated field in the h- and E planes will be given by these functions with the appropriate scaled time coordinates. When the voltage waveform applied to the IRA feed is not an ideal step, we must convolve the above results with the derivative of the applied voltage.

To verify that these results are consistent the boresight results presented earlier by Baum [1], [12] we must ensure that (15) and (16) agree with (1) as $\theta \to 0$. Farr and Baum verified this for a two-wire feed structure [14], but we verify it here for an arbitrary TEM feed. Comparison of (15) and (16) with (1) with an ideal step excitation produces

$$\lim_{\theta\to 0} \frac{cf_g \cot\theta}{h_a} \Phi^h \left(-\frac{ct'}{\sin\theta}\right) = \delta(t') \tag{18}$$

in the H plane and

$$\lim_{\theta\to 0} \frac{cf_g}{h_a \sin\theta} \Phi^e \left(-\frac{ct'}{\sin\theta}\right) = \delta(t') \tag{19}$$

in the E plane. In order for (18) and (19) to be true, we must show that the function approaches infinity as $t' \to 0$ and that the integrated area is unity in the limit $\theta \to 0$. The left-hand-sides of both (18) and (19) clearly approach infinity at $t' = 0$ in the limit $\theta \to 0$. We evaluate

$$\lim_{\theta\to 0} \int_{-\infty}^{\infty} \frac{cf_g}{h_a} \frac{\cos\theta}{\sin\theta} \Phi^h \left(-\frac{ct'}{\sin\theta}\right) dt' = \frac{cf_g}{h_a} \lim_{\theta\to 0} \frac{1}{\sin\theta} \times \int_{-x_{\max}\frac{\sin\theta}{c}}^{x_{\max}\frac{\sin\theta}{c}} \int_{y_{\min}}^{y_{\max}} E_y \left(-\frac{ct'}{\sin\theta}, y\right) dy dt' = I_h \tag{20}$$

where $x_{\max}$ is the maximum horizontal extent of the focused aperture. Making the change of variables $x = -ct'/\sin\theta$, (20) reduces to

$$I_h = \frac{f_g}{h_a} \iint_A E_y(x,y) dx dy = 1. \tag{21}$$

Equation (21) was simplified using (2). A virtually identical analysis of (19) produces

$$I_e = \lim_{\theta\to 0} \int_{-\infty}^{\infty} \frac{cf_g}{h_a} \frac{1}{\sin\theta} \Phi^e \left(-\frac{ct'}{\sin\theta}\right) dt' = \frac{f_g}{h_a} \iint_A E_y(x,y) dx dy = 1. \tag{22}$$

B. Cross-Polarized Fields

A similar analysis can be carried out for the cross-polarized radiated fields, resulting in almost the same results. The cross-polarized radiation in the H plane is a function of the integral

$$E_\phi^h(r,\theta,t) \propto \int_{y_{\min}}^{y_{\max}} E_x \left(-\frac{ct'}{\sin\theta}, y'\right) dy' \tag{23}$$

and the cross-polarized radiation in the E plane is a function of the integral

$$E_\theta^e(r,\theta,t) \propto \int_{x_{\min}}^{x_{\max}} E_x \left(x', -\frac{ct'}{\sin\theta}\right) dx'. \tag{24}$$

The integral in (23) is equivalent to the difference in magnetic scalar potential at the top and bottom of the aperture at horizontal position $x = -ct'/\sin\theta$, and the integral in (24) is equivalent to the difference in electric scalar potential at the left and right edges of the aperture at vertical position $y = -ct'/\sin\theta$. Due to symmetry considerations, the integral in (24) is zero. The integral in (23) is an order of magnitude (or more) smaller than the corresponding integral in (14) because the TEM modes of typical IRA feeds are predominantly in the y direction. Experimental evidence indicates that other factors such as manufacturing defects and diffraction from the edge of the aperture and the feed arms dominates the cross-polarized fields [7]. These features are beyond the scope of this study.

III. Frequency Domain Sidelobe Patterns

To find the sidelobes as a function of θ for a given frequency ω, we take the Fourier transforms of (15) and (16) to get

$$E_\phi^h(r,\theta,\omega) = \frac{V_0 \cos\theta}{2\pi r c} \tilde{\Phi}^h \left(-\frac{\omega \sin\theta}{c}\right) \tag{25}$$

and

$$E_\theta^e(r,\theta,\omega) = \frac{V_0}{2\pi r c} \tilde{\Phi}^e \left(-\frac{\omega \sin\theta}{c}\right). \tag{26}$$

In the above equations, $\tilde{\Phi}(k)$ is the Fourier transform of $\Phi(x)$. We can finally compute the effective gain in the E and H planes by dividing the local radiated power density given by (25) and (26) by the average power density that would exist were all the power *available* to the antenna to be radiated isotropically.[1] The total power spectral density available to the antenna is equal to the power spectral density launched on the feed line. Assuming step excitation this is

$$P_{\text{tot}}(\omega) = \frac{1}{2\omega^2 Z_{\text{line}}} [\text{J/Hz}] \tag{27}$$

and the gain is

$$G^{(h)}(\theta,\omega) = 4\pi \cos^2\theta f_g \frac{f^2 \left|\tilde{\Phi}^{(h)}\left(-\frac{\omega\sin\theta}{c}\right)\right|^2}{c^2} \tag{28}$$

and

$$G^{(e)}(\theta,\omega) = 4\pi f_g \frac{f^2 \left|\tilde{\Phi}^{(e)}\left(-\frac{\omega\sin\theta}{c}\right)\right|^2}{c^2}. \tag{29}$$

By examining the Fourier transforms of Φ^e and Φ^h for the various configurations of interest, we can determine the sidelobe performance in each case. These distributions are presented in Fig. 6 and Fig. 7 for the 45° and 60° feed arms, respectively. Equation (29) tells us that the antenna pattern *shape* is independent of frequency in the E plane, and (28) says that the shape in the H plane is invariant, except for an overall envelope weighting of $\cos^2\theta$. This is because the aperture illumination is identical for all frequencies (since the feed is TEM). The only change

[1]Note, this definition of effective gain differs from the standard definition of directivity. Directivity only considers average *radiated* power. Effective gain and directivity would be equal if *all available* power were radiated by the antenna at all frequencies, which is of course not realistic.

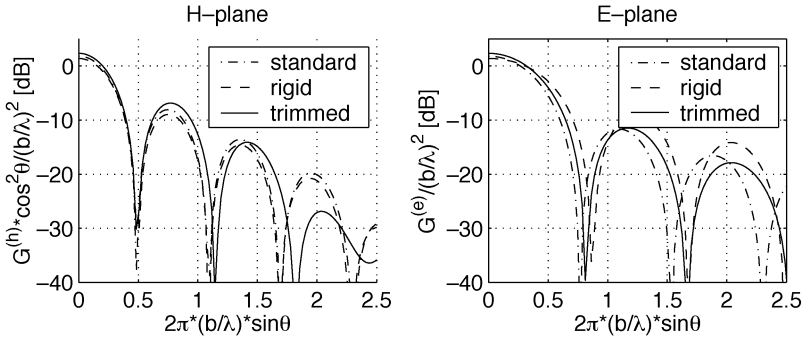

Fig. 6. Sidelobe patterns for the 45° feed arms in the E and H planes. These curves are obtained by taking the Fourier transforms of Φ^h and Φ^e presented in Fig. 4. The gain is normalized to the size of the aperture (in wavelengths) squared as discussed in the text. For example, to get the gain for an aperture that has a maximum radius of one wavelength, add 8.2 dB.

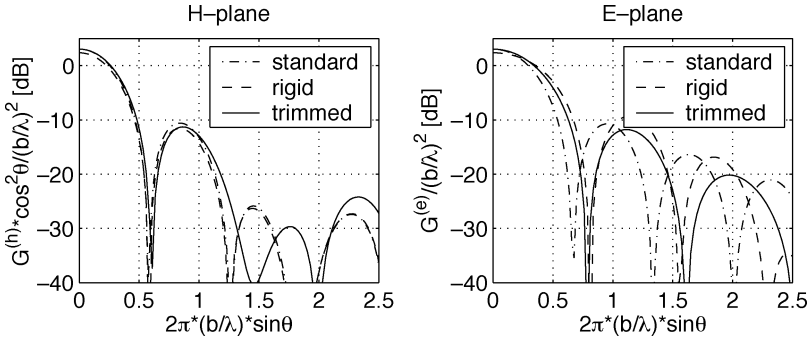

Fig. 7. Sidelobe patterns for the 60° feed arms in the E and H planes. These curves are obtained by taking the Fourier transforms of Φ^h and Φ^e presented in Fig. 5. The normalization is described in the caption to Fig. 6.

as a function of frequency is the *location* in angular space of the sidelobes. The key features of the sidelobe patterns are presented in Table I.

We see from the table that the 60° configurations all provide approximately 1 dB of additional peak gain, depending on the configuration of the aperture. A 1 dB increase in gain corresponds to a 10% increase in the radiated electric field. These results agree with previous numerical [6] and experimental [7] studies. We also see that the average sidelobe levels (SLL) are significantly reduced for the 60° feed arms, especially in the H plane, where we see a 4–5 dB reduction in SLL. This reduction in sidelobes comes at the expense of a larger beamwidth.

Knowledge of Φ^h and Φ^e allows us to predict the antenna radiation pattern as a function of both angle and frequency. Example radiation patterns are presented for the 200 Ω trimmed configurations with $\phi_0 = 45°$ and $\phi_0 = 60°$ in Fig. 8 and Fig. 9, respectively [15]. It is evident in Fig. 8 that the shape of the radiation pattern is fixed as a function of frequency. Only the relative width of the pattern decreases.

TABLE I
SIDELOBE PERFORMANCE, GAIN, AND 3 dB BEAMWIDTH. EFFECTIVE GAIN IS NORMALIZED TO THE SIZE OF THE APERTURE IN WAVELENGTHS. IN MOST CASES, THE FIRST SIDELOBE IS THE LARGEST. HOWEVER, IN SOME CASES THE SECOND SIDELOBE IS LARGER THAN THE FIRST. THE SIDELOBE LEVELS ARE GIVEN RELATIVE TO THE PEAK GAIN IN THE MAIN LOBE

ϕ_0	ap.	$\frac{G}{(a/\lambda)^2}$	H-plane		E-Plane	
			SLL	BW	SLL	BW
°		dB	dB down	°	dB down	°
45	S	3.55	-9.90	4.71	-13.5	6.82
45	R	3.12	-10.3	4.41	-10.56	8.86
45	T	4.08	-9.2	4.41	-13.83	7.37
60	S	4.78	-13.7	5.00	-13.8	5.78
60	R	4.10	-14.0	5.40	-11.7	7.87
60	T	4.78	-14.3	5.40	-14.9	6.89

IV. EXPERIMENTAL MEASUREMENTS

A set of experimental measurements was collected using a half-IRA. A half-IRA is an IRA where the bottom half of the reflector and feed shown in Fig. 1 is replaced by a ground plane. Ideally this ground plane should be infinite, and image theory predicts that the performance of the half IRA would be identical to that of the full IRA. In practice, the ground plane must be finite, and this affects the late-time behavior of the antenna. Half-IRAs have the distinct advantage over IRAs in that there is no need for a balun if the antenna is to be fed with an unbalanced feed, e.g. a coaxial feed structure. Instead, the transition can be made at a "point" or using a feed-point lens. Even with a truncated ground plane, the feed impedance and aperture height for a Half-IRA is half that of the corresponding full IRA. The early-time response of the half-IRA is predicted by (1) and (2), just as for the full IRA. The prompt off-boresight fields are predicted by (15) and (16), with the appropriate forms of $\Phi^h(x)$ and $\Phi^e(x)$.

The half-IRA used in this study was a 100-Ohm configuration with $\phi_0 = 45°$. The diameter of the half-IRA was 1 m. The aperture was untrimmed, resulting in the "standard" aperture configuration of Fig. 2. The data were obtained directly in

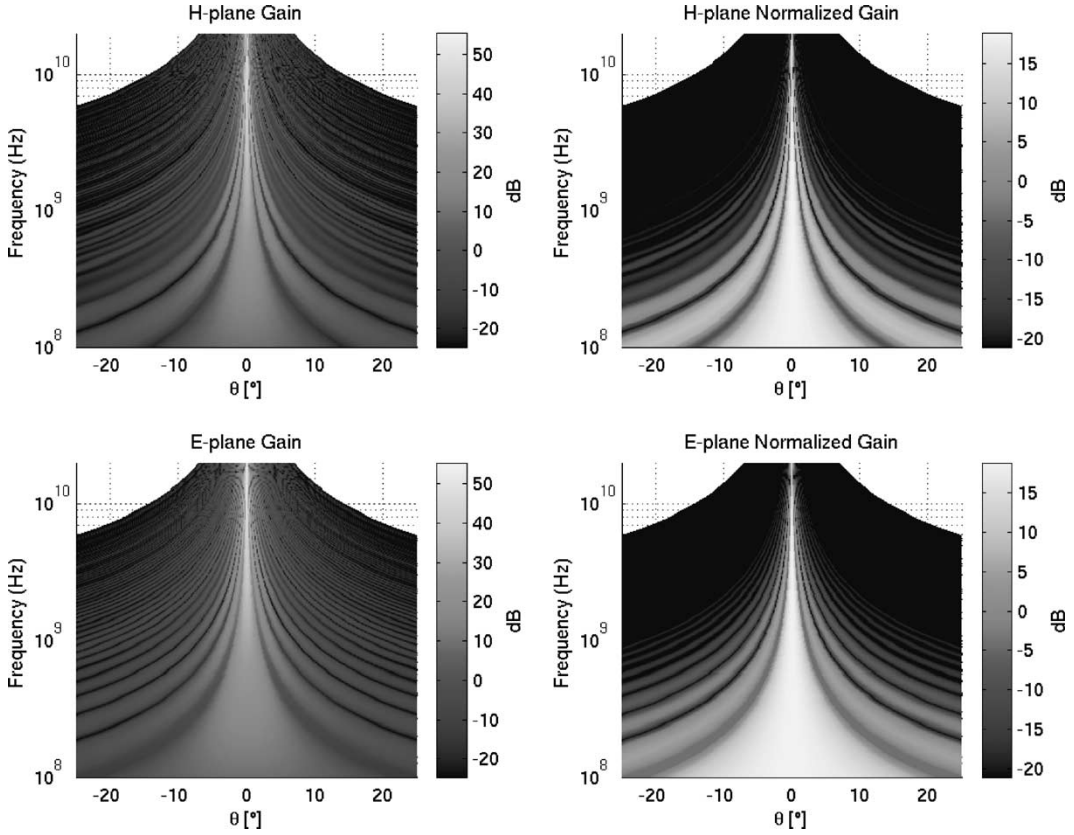

Fig. 8. Absolute gain (left column) and wavelength normalized gain (right column) for the trimmed aperture configuration with $\phi_0 = 45°$. Wavelength normalized gain is obtained by normalizing the value of the gain to $(\lambda/b)^2$. In the absolute gain plot, it is clear that the gain increases for higher frequencies (as f^2). Gain is computed for a 1-m diameter aperture. Increasing the size of the aperture will increase the gain and change the location of the peaks as shown in figures Fig. 6 and Fig. 7.

the time domain using a TEM sensor with 2-ns clear time. The sensor used was a "replicating probe" with an output voltage that is a replica of the incident E field waveform for the clear time of the sensor [16], [17]. The sensor was not absolutely calibrated, i.e., the sensitivity (effective height) of the sensor was not directly measured.

The antenna was fed with a picosecond pulse labs 4015C pulser, which produced a -4 V amplitude step-like waveform with a 15 ps rise time. The effective rise time of the waveform on the antenna (taking into account the cables and connections) was approximately 22 ps. Data was measured with a Tektronix CSA 803A communications signal analyzer equipped with an SD-24 20-GHz sampling head. The effective sampling interval of this device is 0.5 ps.

The two antennas were positioned on camera tripods 26.6 m apart. The measurements were made outside over an arroyo (a dry creek bed) that delayed the ground-bounce signal, i.e., the reflected signal from the flat ground that appears delayed in time. The half IRA was then rotated in the E and H planes to obtain off-boresight measurements. The sensor was fixed throughout and oriented toward the feed point of the half-IRA. For experimental convenience, the pulser was actually connected to the sensor and the sampling head to the half IRA, but reciprocity guarantees that interchange of source and receiver produces identical results. The measured responses are presented in Fig. 10 in the H and E planes, and compared with the predictions made using (15) and (16).

The data presented in Fig. 10 are normalized E field values. Because the absolute sensitivity of the sensor was uncalibrated, only relative comparisons could be made among the different off-boresight angles. To facilitate a comparison between the measured and predicted response, the measured data was normalized to the peak boresight measured field, and the predicted data was normalized to the peak boresight predicted fields. It is known that (1) and (2) tend to over predict the peak fields on boresight for reflector IRAs, possibly due to feed blockage that is ignored in the geometric optics approximations used to derive (1) and (2) [1], [8].

V. Discussion

Figs. 8 and 9 demonstrate some of the important features of the radiation pattern from IRAs. First, we see from the unnormalized gain plots that the peak boresight gain increases as f^2, as is the case for all ideal aperture antennas at high frequencies. This is predicted by (1), which has a time derivative of the applied voltage (equivalent to multiplying by $j\omega$ in the frequency domain). It is important to note that IRAs, like other aperture antennas *are not constant gain*. However, when excited by an ideal step function (which has energy content which varies like $1/f^2$, the radiated field is (approximately) impulsive. While the absolute gain does increase as f^2, the shape of the sidelobe patterns are *independent* of frequency. This uniformity is due to the ultrawide-bandnature of the feed structure. The aperture fields

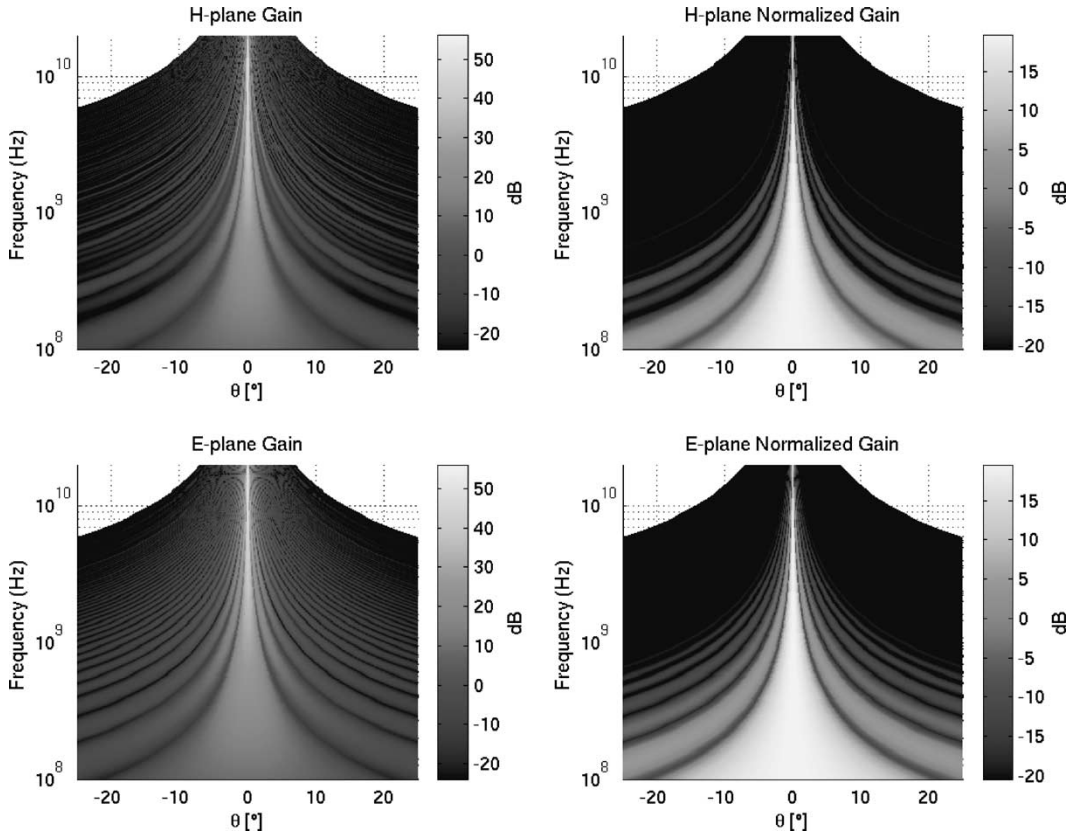

Fig. 9. Absolute gain (left column) and wavelength normalized gain (right column) for the trimmed aperture configuration with $\phi_0 = 60°$. See caption of Fig. 8 for definition of wavelength normalized gain.

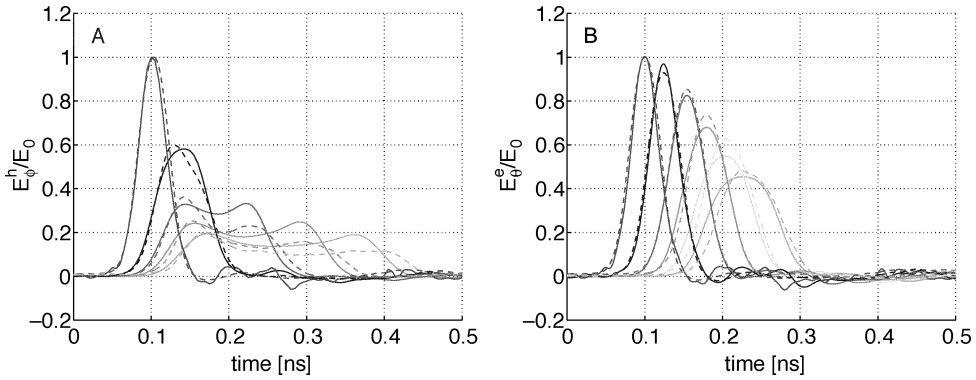

Fig. 10. Measured (dashed) and predicted (solid) E field in the H plane (a) and the E plane (b). The peak field decreases monotonically off-boresight in both cases. Measurements and predictions were made at $\theta = 0°$, 1.25°, 2.5°, 3.75°, and 5° in the H plane ($\phi = 0°$). Measurements and predictions were made at $\theta = 0°$, 1.2°, 2.2°, 3.2°, 4.2°, and 5.2° in the E plane ($\phi = 90°$).

are identical due to the ultrawide-band nature of the feed structure for all frequencies, so long as the higher order modes are insignificant.

The aperture field distributions in TEM-horn fed IRAs can cause higher sidelobe levels than more conventional feeds. Conventional waveguide horn-fed aperture antennas usually have smoothly varying aperture distributions with a single peak in the center of the aperture. In contrast, the dominant mode field distributions for certain TEM feeds can have multiple local peaks that produce higher sidelobe levels and reduce the overall aperture efficiency. This is clearly demonstrated by the data in Table I. With feed arms at 45°, the sidelobes are actually *worse* than for a uniformly illuminated aperture. The presence of the feed arms causes $\Phi^h(x)$ to be peaked away from the center, giving rise to high sidelobe levels. The problem is less severe in the E plane, because Φ^e is smooth and unimodal, i.e., it is shaped more like a conventional aperture distribution. In contrast, Φ^h is much less peaked with $\phi_0 = 60°$, resulting in the lower sidelobe levels shown in Table I.

The measured and predicted data presented in Fig. 10 have good qualitative agreement, though there are noticeable differences. The relative values of the peak fields and FWHM pulse widths are well predicted by (15) and (16), though there are some shape differences between the predicted and measured waveforms. Fig. 11(a) presents the peak measured and predicted fields and Fig. 11(b) presents the measured and

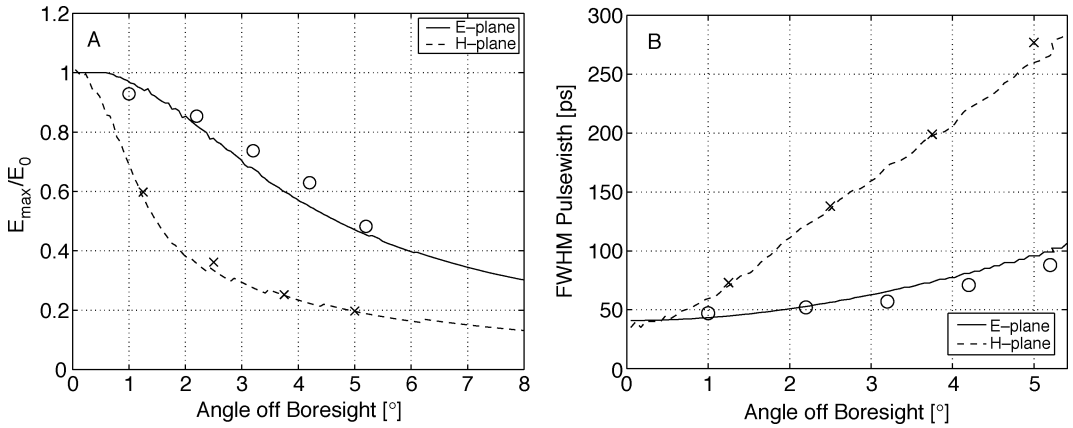

Fig. 11. Predicted (curves) and measured (data points) values of the (a) normalized peak radiated fields and (b) FWHM pulse widths in the H plane (solid, o) and E plane (dashed, x). Evaluation of (15) and (16) for angles less than $\approx 0.5°$ was problematic due to the required sampling resolution for $\Phi^h(x)$ and $\Phi^e(x)$. Measured data was normalized to the peak boresight measured fields, and predicted data was normalized to the peak boresight predicted fields. Boresight predictions were made using (1), (18), and (19).

predicted FWHM pulse widths. In the H plane the agreement is excellent for both pulse width and peak radiated field (<8% error for all cases). In the E plane, the trend is accurately predicted, but the agreement is not as good as in the H plane. The boresight response was predicted using (1) rather than the limiting form of (15) or (16).

The general shape of the waveform in the H plane with two peaks as seen in Fig. 10(a) is predicted by (15), though the asymmetrical shape of the measured response is not predicted. The reduced amplitude of the second peak is likely due to asymmetric feed blockage and defocus across the aperture. On boresight, the feed arms are very thin and are ignored in deriving the prompt response in (1) and (2). Off-boresight, the effect of the feed arms must be reintroduced, causing perturbations in the theory presented here. In the past, a geometric optics treatment has been used to treat feed blockage by removing the portions of the aperture obstructed by the feed arms. However, the feed arms typically used with reflector IRAs have very small projected areas, even for off-boresight angles. A full-wave analysis of the effect of feed blockage is therefore warranted. A second mechanism that can produce the asymmetric H plane response is defocus. Preliminary results indicate that when the electrical feed and the optical focus are not exactly coincident, the first peak of the transient response in the H plane is larger than the second [7]. The subject of prompt and late-time feed blockage in IRAs is a topic for future investigation. In addition, the model does seem to slightly over estimate the initial rise time of the off-boresight waveforms. In the E plane, both the model and the measurements indicate a unimodal waveform. As discussed above, the numerical implementation of the model predicts anomalously high response at angles less than approximately 1.5°. At larger angles, (16) seems to predict broader pulses than were measured. Both (15) and (16) seem to slightly over predict the initial rise time of the radiated fields, though they both do quite well at predicting the fall time.

VI. Conclusion

In this paper, we presented a physical optics theory for the time-domain, off-boresight radiated fields of IRAs. We used the theory to predict and compare the sidelobe performance of common reflector IRAs with feed arms at 45° and 60° from the horizontal. The theory indicates that the sidelobe performance of the 60° IRA is significantly better than the 45° IRAs. When coupled with earlier results that demonstrate a significant improvement in boresight gain [6], [7] and cross polarization performance [7] for the 60° IRAs, it is clear that reflector IRAs with 60° feed arms are an improvement over the more traditional 45° IRAs.

The theoretical predictions were compared with measured data in the far-zone of a 1-m diameter half IRA with feed arms at 45°. Both theory and experiment indicate that the prompt radiated field in the H plane has two peaks, while the radiated field in the E plane has only one. The experimental measurements indicate asymmetries in the temporal response in the H plane which are not apparent in the theoretical data. We hypothesize that this might be due to asymmetric feed blockage off boresight, as the theory presented here completely neglects feed blockage.

References

[1] C. E. Baum, E. G. Farr, and D. V. Giri, "Review of impulse-radiating antennas," in *Review of Radio Science*, W. R. Stone, Ed. Oxford, U.K.: Oxford Univ. Press, 1999, pp. 403–439.

[2] W. R. Smythe, *Static and Dynamic Electricity*, 3rd ed. Bristol, PA: Taylor and Francis, 1989.

[3] C. E. Baum, "Aperture efficiencies of IRAs," in *Sensor and Simulation Notes #328*, C. E. Baum, Ed. Albuquerque, NM: Phillips Lab., 1991.

[4] C. J. Buchenauer, J. S. Tyo, and J. S. H. Schoenberg, "Prompt aperture efficiencies of impulse radiating antennas with arrays as an application," *IEEE Trans. Antennas Propagat.*, vol. 49, pp. 1155–1165, Aug. 2001.

[5] M. J. Baretela and J. S. Tyo, "Improvement of prompt radiated response from impulse radiating antennas by aperture trimming," *IEEE Trans. Antennas Propagat.*, vol. 51, pp. 2158–2167, Sept. 2003.

[6] J. S. Tyo, "Optimization of the TEM feed structure for four-arm reflector impulse radiating antennas," *IEEE Trans. Antennas Propagat.*, vol. 49, pp. 607–614, Apr. 2001.

[7] L. H. Bowen, E. G. Farr, C. E. Baum, T. C. Tran, and W. D. Prather, "Experimental results of optimizing the location of feed arms in a collapsible IRA and a solid IRA," in *Sensor and Simulation Notes #450*, C. E. Baum, Ed. Albuquerque, NM: Air Force Research Lab., 2000.

[8] D. V. Giri, H. Lackner, I. D. Smith, D. W. Morton, C. E. Baum, J. R. Marek, W. D. Prather, and D. W. Scholfield, "Design, fabrication, and testing of a paraboloidal reflector antenna and pulser system for impulse-like waveforms," *IEEE Trans. Plasma Sci.*, vol. 25, pp. 318–326, Apr. 1997.

[9] L. H. Bowen, E. G. Farr, J. P. Paxton, A. J. Witzig, C. E. Baum, D. I. Lawry, and W. D. Prather, "Fabrication and testing of a membrane IRA," in *Sensor and Simulation Notes #464*, C. E. Baum, Ed. Albuquerque, NM: Air Force Research Lab., 2002.

[10] L. M. Atchley, E. G. Farr, J. S. Tyo, N. de la Merced, and L. L. Altgilbers, "Development and testing of a parachute deployable impulse radiating antenna," in *Sensor and Simulation Notes #465*, C. E. Baum, Ed. Albuquerque, NM: Air Force Research Lab., 2002.
[11] J. S. Tyo, E. G. Farr, L. H. Bowen, and L. Altgilbers, "IRA variations useful for flexible feed arm," in *Sensor and Simulation Notes #472*, C. E. Baum, Ed. Albuquerque, NM: Air Force Research Lab., 2002.
[12] C. E. Baum, "Focused aperture antennas," in *Sensor and Simulation Notes #306*, C. E. Baum, Ed. Albuquerque, NM: Air Force Weapons Lab., 1987.
[13] C. A. Balanis, *Advanced Engineering Electromagnetics*. New York: Wiley, 1989.
[14] E. G. Farr and C. E. Baum, "Radiation pattern of reflector impulse radiating antennas: early time response," in *Sensor and Simulation Notes #358*, C. E. Baum, Ed. Albuquerque, NM: Phillips Lab., 1993.
[15] C. Rappaport, "A colormap for effective black and white rendering of color-scale images," *IEEE Antennas and Propagat. Mag.*, vol. 44, pp. 94–96, June 2002.
[16] C. J. Buchenauer, J. S. Tyo, and J. S. H. Schoenberg, "Antennas and electric field sensors for ultra-wideband transient measurements: applications and methods," in *Ultra-Wideband, Short-Pulse Electromagnetics 3*, C. E. Baum, L. Carin, and A. P. Stone, Eds. New York: Plenum, 1997, pp. 405–421.
[17] E. G. Farr, C. E. Baum, and W. D. Prather, "Multifunciton impulse radiating antennas: theory and experiment," in *Sensor and Simulation Notes #413*, C. E. Baum, Ed. Albuquerque, NM: Air Force Research Lab., 1997.

J. Scott Tyo (S'94–M'96) was born at the Frankfurt American Hospital in 1972. He received the BSE, MSE, and Ph.D. degrees in electrical engineering from the University of Pennsylvania, Philadelphia, in 1994, 1996, and 1997, respectively.

He is an Assistant Professor in the Electrical and Computer Engineering Department, University of New Mexico (UNM). From 1994 to 2001, he was an Officer in the U.S. Air Force, leaving service at the rank of Captain. From 1996 to 1999, he was a Research Engineer in the Directed Energy Directorate, USAF Research Laboratory, Kirtland AFB, NM. From 1999 to 2001, he was a Member of the faculty of the ECE department, U.S. Naval Postgraduate School, Monterey, CA. He joined the faculty at UNM in 2001. Since joining UNM, his research has focused on ultrawide-band microwave radiating systems as well as microwave and optical remote sensing.

Prof. Tyo is a Member of Tau Beta Pi, and Eta Kappa Nu, the Optical Society of America (OSA), Washington, DC, the International Scientific Radio Union (URSI) Commissions B and E, and The International Society for Optical Engineers (SPIE), Bellingham, WA.

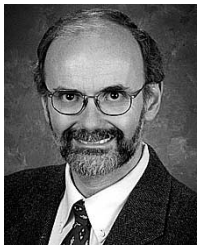

Everett G. Farr (S'82–M'86–SM'01) received the B.S. degree in physics and the M.S. and Ph.D. degrees in electrical engineering all from the University of Illinois at Urbana-Champaign, in 1980, 1982, and 1985, respectively.

From 1985 to 1989, he was with BDM International, where he worked on a variety of problems dealing with electromagnetic pulse and high power microwaves. From 1989 to 1991, he was with Electromagnetic Applications, Inc., where he worked on numerical methods for EMP, and where he began his investigation of IRAs. In 1991, he formed Farr Research, Incorporated, Albuquerque, NM, and is currently the President. Here, he has developed and optimized ultrawide-band IRAs in a number of configurations. These include IRAs with aluminum reflectors, collapsible IRAs with fabric reflectors, IRAs for space deployment, IRAs mounted onto a parachute, and IRAs for high-voltage applications. He also worked on time domain antenna measurement techniques, and he has developed the Portable Automatic Time-domain Antenna Range (PATARTM) system.

Dr. Farr is a Member of Eta Kappa Nu and the International Scientific Radio Union (URSI) Commission E. He won the Best Applied Paper Award at the 1990 Nuclear Electromagnetics Conference. In 2000, he was awarded the honor of Summa Foundation EMP Fellow and the Best Applied Paper at the 2002 AMEREM Conference.

Jon S. H. Schoenberg (M'86–SM'98) was born in Schenectady, NY, in 1963. He received the B.S. degree in electrical engineering from Cornell University, Ithaca, NY, the M.S.E.E. degree from Northeastern University, Boston, MA, and the Ph.D. degree in electrical engineering from the University of Colorado, Boulder, in 1985, 1989, and 1995, respectively.

From 1985 to 1989, he was assigned to the Rome Air Development Center, where he developed MMICs for phased arrays and performed high-speed photoconductive semiconductor switching research. From 1989 to 1992 and 1999 to 2002, he served on the faculty of the U.S. Air Force Academy, Colorado Springs, CO, first as Instructor, then later as Associate Professor of electrical engineering. From 1992 to 1995, he was at the University of Colorado, performing research on microwave transmission-wave power combining arrays under an Air Force Institute of Technology fellowship. From 1995 to 1999, he was assigned to the Directed Energy Directorate of the Air Force Research Laboratory, Kirtland AFB, where he developed solid-state sources and antennas for ultrawide-bandelectromagnetic applications. Since 2002, he has been a Program Manager with the U.S. Department of Defense responsible for executing research and development projects across the uniformed services.

Major Schoenberg is a Registered Professional Engineer. He is a Member of Tau Beta Pi, Eta Kappa Nu, and the International Scientific Radio Union (URSI).

Leland H. Bowen received the B.S.E.E. degree (*magna cum laude*) from the University of New Mexico, Albuquerque, and the M.S.E.E. degree from Arizona State University, Tempe, in 1965 and 1968, respectively.

From 1970 to 1983, he was a manufacturing Jeweler and vocational Instructor. In 1983, he joined Electromagnetic Applications, Inc., Albuquerque, NM, where he specialized in numerical modeling of electromagnetic nuclear effects. From 1992 to 1997, he was Senior Engineer at Shield-Rite, Inc., Albuquerque. In 1998, he joined Farr Research, Inc., Albuquerque, as a Senior Research Engineer. He currently specializes in UWB antenna research and development.

Mr. Bowen is a licensed Professional Engineer in the state of New Mexico.

Larry L. Altgilbers (M'01) received the Ph.D. degree in physics from the Semiconductor Physics Institute, Vilnius, Lithuania, where he did research on explosive pulsed power.

From 1976 until 1991, he was employed by the U.S. Army Aviation and Missile Command where he worked on directed energy weapons and various missile systems. Since 1991, he has been employed by the U.S. Army Space and Missile Defense Command, where he initially worked on directed energy weapons and is now in the Advanced Technology Directorate, Redstone Arsenal, AL. His current duties include managing the development of a variety of technologies through the Small Business Innovative Research Program and the development of pulsed power and radio frequency technologies. He authored *Magnetocumulative Generators (High Pressure Shock Compression of Condensed Matter* (New York: Springer Verlag; March 2000) and was a contributing author to *Jane's Unconventional Weapons Handbook* (Washington, DC: Jane's Information Group, 2000) and over 50 conference and journal publications.

Dr. Altgilbers is a Member of the American Physical Society, and the American Institute of Aeronautics and Astronautics.